Nanoscale

RSC Publishing

PAPER

View Article Online
View Journal | View Issue

Cite this: *Nanoscale*, 2013, **5**, 5009

Highly ordered monolayer/bilayer TiO_2 hollow sphere films with widely tunable visible-light reflection and absorption bands†

Jie Li,‡[a] Yao Qin,‡[b] Chao Jin,[a] Ying Li,[a] Donglu Shi,[b] Lukas Schmidt-Mende,[d] Lihua Gan*[a] and Jinhu Yang*[abc]

Received 13th February 2013
Accepted 3rd April 2013

DOI: 10.1039/c3nr00778b

www.rsc.org/nanoscale

Monolayer and bilayer TiO_2 hollow hemisphere/sphere (THH/THS) films consisting of highly ordered hexagonal-patterned THHs/THSs with thin shells of ~10 nm and different diameters of ~170 and ~470 nm have been prepared by templating of two-dimensional polystyrene sphere (PS) assembly films coupled with TiO_2 sputtering/wet coating approaches. Owing to their precisely adjustable structural parameters, such as THH/THS shape and diameter as well as film layer thickness, the prepared THH/THS films exhibit widely tunable visible-light reflection and absorption bands, *i.e.* from 380 to 850 nm for reflection and 390 to 520 nm for absorption, respectively. The mechanism of the novel optical behaviors of the THH/THS films has been discussed in depth, combined with some calculations according to Bragg's law. In addition, photocatalytic experiments of RhB degradation employing the THH/THS films as recyclable catalysts have been conducted. The THH/THS films with controlled structures and precisely tunable optical properties are attractive for a wide range of applications, such as recyclable catalysts for photocatalysis, efficient oxide electrodes or scattering layers for solar cells, gas-permeable electrode materials for high-performance sensors and so on.

1 Introduction

TiO_2 has emerged as one of the most important semiconductors due to its unique properties such as high reactivity, chemical stability and long-term photostability, and great potential in the area of photocatalysis,[1–3] energy conversion and storage[4–8] as well as sensors,[9,10] self-cleaning surfaces[11,12] and pigments.[11,13,14] Nanostructured TiO_2 films deposited on necessary substrates have attracted great attention because they are essential device components for most practical applications. In order to acquire higher performance, a variety of TiO_2 films with purpose-designed nanostructures such as TiO_2 nanorod/nanowire/nanotube arrays,[5,6,15] intercrossing piled logs,[16] and ordered hollow sphere[17–22] and inverse opal[23,24] structures have been prepared as key components for photovoltaic and photocatalytic investigations. Among these, one particular focus has been on TiO_2 hollow sphere (THS) films due to their unique properties such as relatively high specific surface area, efficient light scattering and trapping capacity, synthetic feasibility and high mobility for easy and stable film assembly, which are attractive for related photoelectric applications.[25–27] So far, THS films with different layers have been fabricated by, mostly, templating of polystyrene sphere (PS) films coupled with subsequent TiO_2 coating and template removal processes.

Generally, PS film templates for THS synthesis were realized by two main approaches coupled with a self-assembly technique, *i.e.*, either spin coating for monolayer films[17] or vertical deposition for multiple layer films.[28] For example, monolayer/multiple layer PS films have been prepared through these approaches and utilized as effective templates to produce shape-preserved THS films which worked as oxide electrodes[17,20] or scattering layers[18] for dye sensitized solar cells. However, the PS templates and replicated THS films prepared in these ways often have problems of uncontrolled film thickness (vertical deposition case) or poor film quality with disorder (spin coating case). It is well recognized that the ordered periodic structure and appropriate thickness of films are key factors for high performance of the devices. Taking solar cells as an example, the ordered structure is crucial for obtaining highly efficient light trapping or scattering, while the appropriate film thickness plays a decisive role in determining carrier transport and collection of the electrode film because electrons have a limit

[a]*Department of Chemistry, Tongji University, Siping Road 1239, Shanghai 200092, People's Republic of China. E-mail: yangjinhu2010@gmail.com, ganlh@tongji.edu.cn*

[b]*Institute for Biomedical Engineering & Nano Science, Tongji University, Siping Road 1239, Shanghai 200092, People's Republic of China*

[c]*Key Laboratory of Yangtze River Water Environment, Ministry of Education, Shanghai 200092, PR China*

[d]*Department of Physics, University of Konstanz, Konstanz, Germany*

† Electronic supplementary information (ESI) available: Raman spectrum and XRD pattern of the THH films (Fig. S1), detailed calculation of reflection and extinction peaks through BL THS film-450 (S1) and multiple views of geometric parameters of BL THS film-450 (Fig. S2). See DOI: 10.1039/c3nr00778b

‡ These authors contributed equally to this work.

diffusion thickness ($L_d = (D \times \tau)^{1/2}$, where L_d, D and τ are diffusion length, diffusion coefficient and lifetime of electrons), which requires an electron-accessible thickness of the electrode films for highly efficient charge collection. Accordingly, the structural uncertainty of replicated THS films can affect light utilization, charge transport and collection, and inevitably lead to drawbacks to the overall efficiency of the film based devices. On the other hand, it is noteworthy that the optical response of THS films shows a critical effect on their photoelectric properties and performance.[18–22] Though a number of reports on THS films have been published, few efforts have been made to investigate the correlations between their optical properties and concrete structures in depth through exquisite experimental design and especially theoretical calculation.

Recently, an air–liquid interface self-assembly (ALIS) method has been reported for preparation of highly ordered monolayer PS film templates and nanostructured inorganic films, such as ZnO nanorod arrays,[29] Ag_2S nanonets,[30] and Co nanodot arrays.[31] However, it has been scarcely applied to TiO_2 materials due likely to high crystallization temperature of TiO_2 that may cause structure collapse of THSs during processes of template removal and TiO_2 crystallization. Herein we demonstrate the facile fabrication of monolayer/bilayer TiO_2 hollow hemisphere/sphere (THH/THS) films with controllable thickness and structures on ITO substrates by the modified ALIS method combined with an improved calcination program, as shown in Scheme 1. The prepared THH and THS films show tunable optical properties such as tunable wide visible-light band reflection and absorption depending merely on the PS size and film layer as well as a means of TiO_2 coating. Calculations on reflection absorption peaks of the representative sample have been conducted and the theoretical results are in good agreement with the measured data. This work offers fundamental significance for nanostructure engineering and optimization of analogous functional films to acquire novel properties and high performance. In addition, the controlled structures with novel properties of the TiO_2 films provide not only promising potential in various related applications, but also a good model to understand in depth the relationship between specific 2D nanostructured films and their optical behaviors.

2 Experimental section

2.1 Preparation of monolayer/bilayer PS assembly films on ITO substrates

PSs used with different diameters (150 nm and 450 nm) were synthesized in laboratory, the surfaces of which were decorated with SO_4^{2-} groups for better TiO_2 adhesion. Preparation of the PS sphere monolayer film on ITO substrates was similar to the method reported previously.[29] In brief, PSs dispersed in a mixed water–ethanol (1 : 1, v/v) solution at certain concentrations (10 g mL^{-1} for 150 nm PSs and 30 g mL^{-1} for 450 nm PSs) were spread on a hydrophilic glass surrounded with water to form a monolayer assembly film on the water surface. Then, the monolayer PS assembly film was picked up by an ITO substrate (1.4 cm × 1.4 cm) to get transferred from the water surface onto the ITO substrate. For bilayer PS films, the monolayer PS assembly film was transferred twice onto the same ITO substrate. Finally the ITOs with monolayer or bilayer PS films were dried in air and kept for further TiO_2 coating onto their surfaces.

2.2 Preparation of TiO_2 hollow sphere films from PS film templates

Two different ways of sputtering and wet coating of TiO_2 onto the PS film on ITO were employed. TiO_2 was sputtered at room

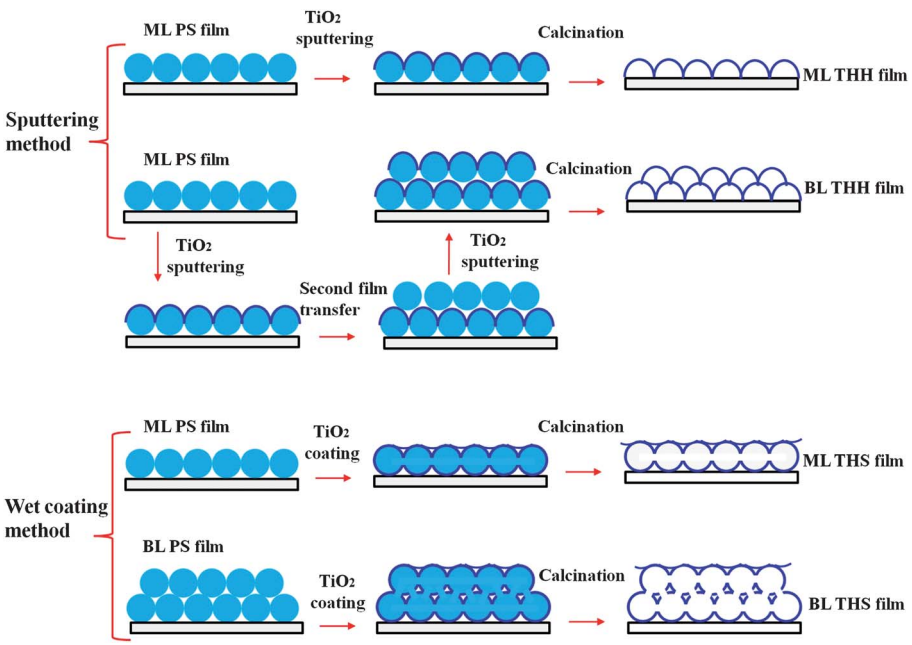

Scheme 1 Schematic illustration of the synthetic routes towards THH and THS films.

temperature with Ar flow (20 sccm) for 10 min utilizing a magnetic-control sputter machine and, alternatively, it was coated onto PS films on vertically standing ITOs by hydrolyzing the titanium isopropoxide (TIP) precursor (0.2 g) in a mixed solution containing 20 mL ethanol and 0.5 mL water for 40 min. It is noted that for the wet coating method ITO supported monolayer or bilayer films were dipped directly in the TIP hydrolysis solution to get TiO_2 coating, while for the sputtering method TiO_2 was sputtered layer by layer, namely, the second PS film was transferred and sputtered after the first monolayer film was sputtered (see Scheme 1 for details). The samples gained from both methods were calcined according to a specially designed program to not only remove PS templates and improve the crystallinity of TiO_2, but also ensure the preservation of the hollow sphere structure from PS film templates. In detail, the samples were annealed following the program with the temperature ramping rate at 1 °C min^{-1} from 25 to 150 °C, and then kept at 150 °C for 6 h to get TiO_2 hollow spheres partly crystallized for self-supporting structures before PS sphere precursors decomposed. Subsequently, the temperature was increased to 480 °C at the same ramping rate of 1 °C min^{-1} and kept at this temperature for 3 h to completely remove PSs and improve the crystallinity of TiO_2.

2.3 Characterization

The morphology of TiO_2 hollow sphere films was characterized using a scanning electron microscope (SEM, Hitachi S4800, 5 kV) and a high-resolution transmission electron microscope (HR-TEM, JEM 2011, 200 kV) together with an energy-dispersive X-ray spectrometer (EDX). The UV-vis reflection and absorption spectra of the samples were recorded on a Hitachi U3501 spectrophotometer.

2.4 Photocatalysis evaluation

The as-prepared THH and THS films as well as the solid TiO_2 film (thickness ~10 nm, prepared by directly sputtering TiO_2 onto a 1.4 cm × 1.4 cm ITO substrate) were immersed in 10 mL of 5 mg L^{-1} rhodamine B (RhB) aqueous solution. After 30 min stirring in the dark with full adsorption of RhB on catalysts, the system was irradiated using a 300 W high-pressure mercury lamp. The samples were taken out from the solution every 30 min and analysed by a UV-vis spectrometer to determine residual RhB in solution. For recyclable photocatalysis, the sample from the previous cycle measurement was washed with water and dried in air for the next cycle.

3 Results and discussion

Fig. 1 presents the typical SEM images of monolayer and bilayer PS films prepared by self-assembly of 450 nm PSs on ITO substrates *via* a modified ALIS method. From an overview image in Fig. 1a, it can be seen that a large-scale assembly film with a smooth surface is formed on the substrate. The edge region (at the bottom left corner) of the film selected purposely shows clearly single layer characteristics, indicating the successful preparation of the monolayer PS film. Fig. 1B shows a high magnification image for close observation, which demonstrates that the monolayer film consists of ~450 nm PSs by ordered self-assembly with a hexagonal symmetry. In addition, as shown in Fig. 1C and D, the ordered bilayer PS film with the same size of PSs and the hexagonal pattern are prepared by transferring monolayer PS films twice onto the ITO substrate. In the low magnification image shown in Fig. 1C, the edge region at the upper left corner also shows that the PS film has a top layer (grey black) and a bottom layer (grey white). The apparent contrast indicates that the bilayer film is formed. This can be seen obviously in another magnified image, Fig. 1D. Then, on the base of these monolayer/bilayer films, the corresponding monolayer/bilayer THH and THS films can be prepared.

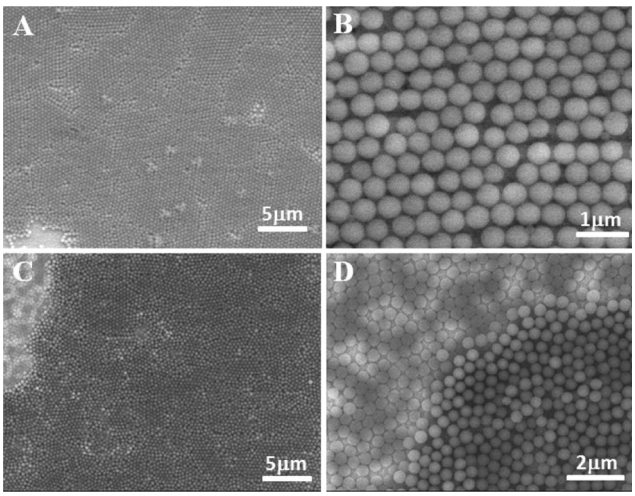

Fig. 1 SEM images of monolayer (A and B) and bilayer (C and D) PS ($d = 450$ nm) films on ITO substrates.

Fig. 2 shows monolayer/bilayer THH films prepared by sputtering TiO_2 onto the PS films following a designed calcination program for template removal and simultaneous TiO_2 crystallization (see Scheme 1 and Experimental section). Fig. 2A and B show an oblique view of the monolayer THH film. As can be seen, the orderly patterned THHs reserve the long-term hexagonal periodicity of the PS film. Compared with the templates of 450 nm PS, the average diameter of the THHs that is estimated to be ~470 nm is relatively large, indicating that the THHs have a very thin shell of ~10 nm. This is well mirrored in the corresponding top-view pictures shown in Fig. 2C and D. Moreover, according to the procedure shown in Scheme 1, bilayer THH films were prepared by layer-by-layer TiO_2 sputtering on transferred PS films. Apparently, the surface of the bilayer THH film looks a little rough relative to the monolayer THH film, as shown in Fig. 2E and F. It is noted that the TiO_2 hollow spheres prepared by the sputtering method are actually hollow hemispheres because the sputtering angle in the sputter system is 45° and the lower half of the PS spheres cannot be sputtered with TiO_2. As a result, the hollow hemispheres were formed when PS sphere templates were removed by calcination.

More information on the structure and composition of the THHs was obtained by TEM, Raman and EDX (Fig. 3). In Fig. 3A, three THHs obtained from the film after sonication treatment

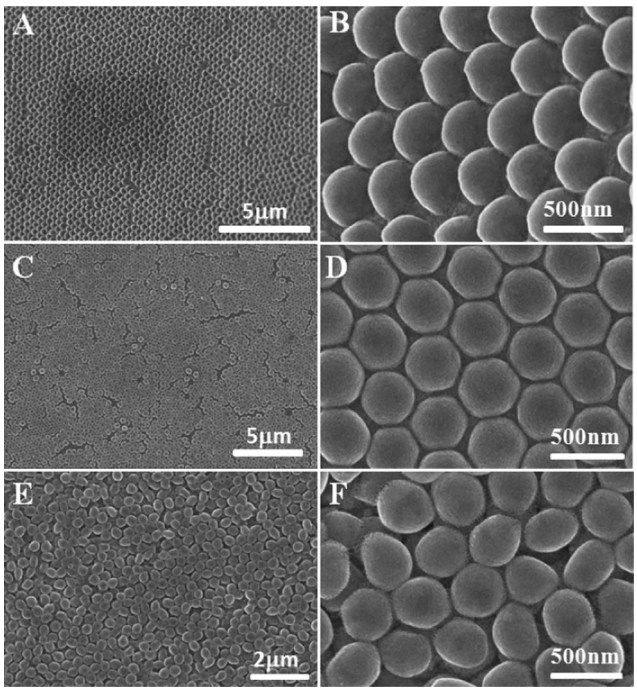

Fig. 2 SEM images of monolayer (A–D) and bilayer (E and F) THH films obtained from 450 nm PS films by a TiO_2 sputtering method.

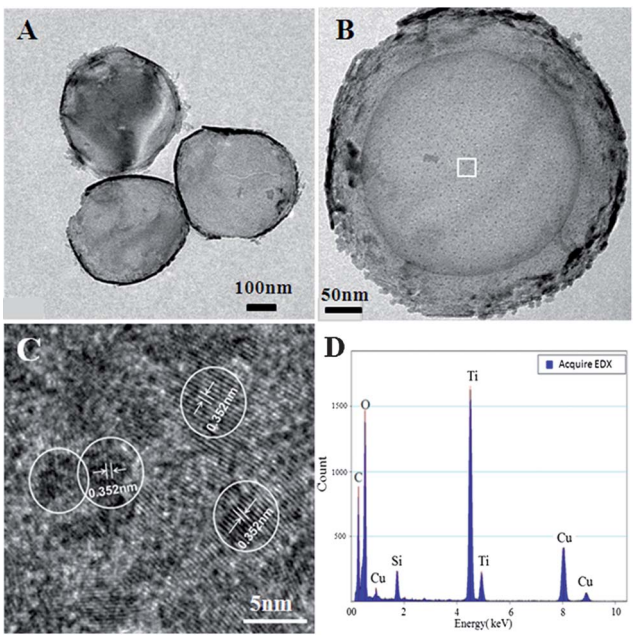

Fig. 3 (A and B) TEM and (C) HRTEM images and (D) EDX pattern of the THHs by templating of 450 nm PSs.

display a typical structure of hollow spheres. From another magnified image shown in Fig. 3B, the diameter and the shell thickness of the THHs are ~470 and 10 nm, respectively, which is in good agreement with the results of SEM observation. At a high resolution, TiO_2 crystallites with diameters of 5–8 nm and clear boundaries are observed. For some crystallites, a set of crystal lattices with *d*-space equivalent to 0.352 nm corresponds to {101} planes of anatase TiO_2. This indicates that the hollow spheres are made of nanosized crystallites and are well crystallized after calcination. The EDS spectrum of the THHs is shown in Fig. 3D, which shows the elements of Ti and O in addition to C, Cu and Si that are thought to be originated from the TEM grid and ITO glass, respectively, suggesting that the hollow spheres are pure TiO_2. In addition, the Raman spectrum of the THH film (Fig. S1a†) shows several peaks at 144, 399, 513 and 639 cm^{-1} corresponding to the typical active modes of anatase TiO_2, *i.e.*, E_g, B_{1g}, A_{1g} and E_g, respectively, confirming that the THHs are in the anatase phase. It is noted that we did find the TiO_2 signal in the corresponding XRD (X-ray diffraction) pattern of the THH films except some peaks generated from ITO glass containing $In_2Sn_2O_{7-x}$ (Fig. S1b†), due to the ultrathin thickness (10–20 nm) of the TiO_2 films that may be beyond the detection limit of the XRD method.

Through similar approaches, monolayer and bilayer THH films consisting of smaller hollow hemispheres were obtained from 150 nm PS film templates, as shown in Fig. 4. It can be seen that the monolayer THH film exhibits highly ordered long-term hexagonal periodicity (Fig. 4A and B), while the bilayer THH film shows a little disorder relatively (Fig. 4C and D), owing to the higher surface energy of the smaller spheres that may activate the displacement of the small spheres from the original location on the rough THH monolayer surface. The replicated THHs have a uniform diameter of ~170 nm and a thin shell of less than 10 nm (insets in Fig. 4A and C).

Alternatively, monolayer and bilayer THS films can be prepared as well from 450 PS film templates by employing a wet coating method for TiO_2 coating. Fig. 5 shows the THS films prepared in solution by directly hydrolyzing Ti precursors of TIP onto the 450 nm monolayer or bilayer PS films. Evidently, the morphologies and structures of the THS films prepared in this method are distinctly different from those by sputtering.

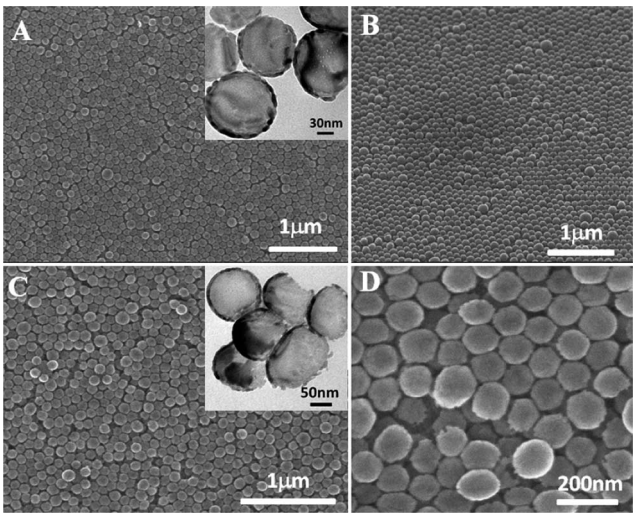

Fig. 4 SEM (A–D) and TEM (insets, B and C) images of monolayer (A and B) and bilayer (C and D) THH films obtained from the 150 nm PS film template through TiO_2 sputtering. The channels between two neighboring hollow spheres in THS films are denoted with red arrows. TiO_2 nanosheets are denoted with blue arrows.

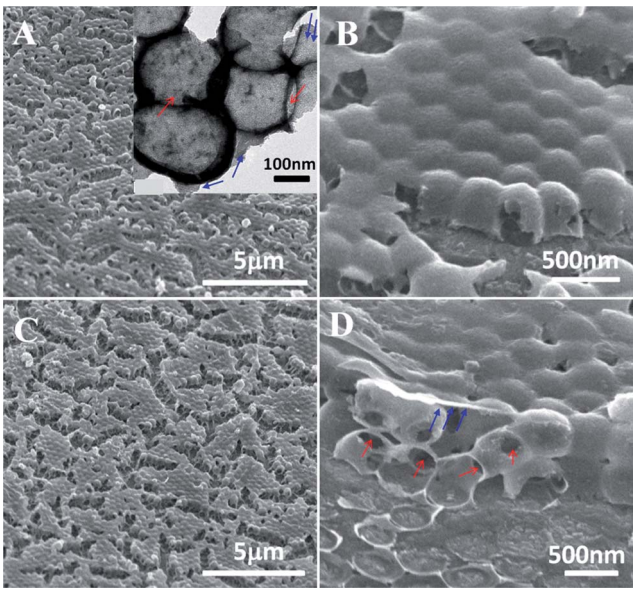

Fig. 5 SEM images of monolayer (A and B) and bilayer (C and D) THS films obtained from 450 nm PS film templates through hydrolysis of TIP followed by calcination. The inset in (A) is the TEM image of the broken TiO_2 hollow spheres obtained by sonication. (B) and (D) are oblique views.

Experimentally, unlike the sputtering method, the PSs can be soaked by TIP precursor solution and fully coated by TiO_2 during hydrolysis, except some contact points between two neighbor PSs, which generate TiO_2 hollow spheres with interconnected channels after PS template removal (see Scheme 1). This is applicable to both cases of the monolayer and bilayer THS film fabrication. The difference, for the monolayer THS film, is that each THS has six channels because each THS is neighbored by six THSs, while for the bilayer THS film, each THS has nine as it is connected by three more THSs from second layers. The channel existence makes the films a little rough (Fig. 5A and C). The channels between two neighbored hollow spheres in monolayer/bilayer THS films are denoted with red arrows, as shown in Fig. 5A (inset) and Fig. 5D. Besides, these THS films are covered by a curved TiO_2 nanosheet (denoted with blue arrows) which is formed possibly by hydrolysis of excess TIP precursor. It can be seen that the thickness of both TiO_2 nanosheets and hollow sphere shells are very thin, which is estimated to be ~10 nm. The novel structure of the THS film with conjoint channels and nanosheet coverage is illustrated in Scheme 1. Compared with the sputtering method, the wet coating method leads to relatively poor disorder of the THS films, due probably to PS falling off when soaked in an TIP hydrolysis solution under stirring, which may affect their reflectance/absorbance spectra more or less. However, the wet method is much simpler and more facile for multiple layer THS film preparation. For example, for bilayer THS film preparation, it needs just one-step soaking to get TiO_2 coating on PS films by the wet coating method, while it needs sputtering twice by the sputtering method. Moreover, as discussed above, the two methods result in different TiO_2 structures, *i.e.* THS films are prepared by the wet coating method, while THH films can only be obtained by the sputtering method.

The optical properties including reflection and absorption of the prepared THH and THS films were investigated systematically. In theory, the position of the measured reflectance peaks through the THH or THS films can be described by Bragg's law:[32,33]

$$m\lambda_{max} = 2n_{avg}d\sin\theta_b \quad (1)$$

where m is an arbitrary integer coefficient ($m = 1, 2, 3, \ldots$), λ is the wavelength of the reflectance peak maximum (*i.e.*, the stopband position), d is the thickness of films, θ_b is the incident Bragg angle and n_{avg} is the average refractive index of anatase TiO_2 and void (air), which is decided by the volume fraction (f) of the TiO_2 material and the void in the films ($n_{avg}^2 = f_{TiO_2} \times n_{TiO_2}^2 + f_{air} \times n_{air}^2$).[34] In this work, all reflectance spectra were recorded at near normal incidence to the surfaces of films, so $\theta_b = 90°$ and $\sin\theta_b = 1$. The films with different layers and THS/THH sizes offer varied refractive indices (n_{avg}) and thickness (d), and thereby are anticipated to give a series of reflectance peaks in the visible light region at appropriate m values. Fig. 6 shows the UV-vis reflection spectra of the films, where intensified reflectance peaks over the full visible-light region are observed with the wavelength ranging widely from the near ultraviolet (380 nm) to near infrared region (850 nm). In addition, the main reflectance peaks of the films show a marked red shift with increasing film thickness (Table 1), for example, ML THS film-150 (410 nm) < BL THH film-150 (445 nm) < ML THH film-450 (470 nm) < BL THH film-450 (480 nm) < ML THS film 450 (540 nm) < BL THS film-450 (620 nm). The shift trend of the reflectance peaks in fact follows eqn (1) that the wavelength of the reflected lights is proportional to the thickness of the films, assuming that n_{avg} for the films is basically constant. As can be seen, almost each sample has multiple (dual or even ternary) reflectance peaks, which indicates that more than one m value satisfies Bragg's law within the measured waveband. The calculations, taking BL THS film-450 as an example, have been conducted for theoretical simulation and comparison (see S1

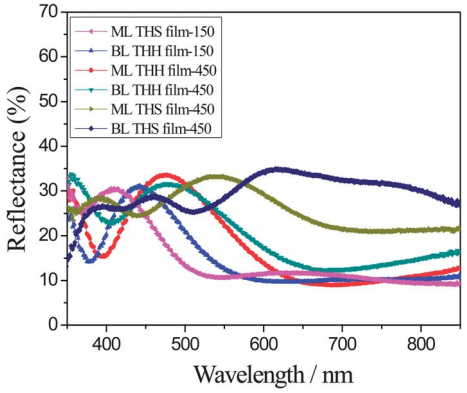

Fig. 6 UV-vis reflection spectra of THH and THS films obtained from PS film templates through two different TiO_2 coating approaches. "ML" and "BL" in the figure refer to monolayer and bilayer, respectively; while 150 and 450 mean THH or THS films are prepared from 150 or 450 nm PS film templates, namely, the diameters of THHs or THSs are ~170 or 470 nm. For example, "ML THH film-150" indicates the monolayer THH film obtained from 150 nm PS film templates.

Table 1 Thickness and reflectance/absorbance peak positions of the prepared THH and THS films

Sample name	Film thickness (nm)	Reflectance peak position (nm)	Absorption peak position (nm)
ML-THS film-150	160	410	<380
BL-THH film-150	168.3	445	<380
ML-THH film-450	235	470	390
BL-THH film-450	465	480	425
ML-THS film-450	470	495, 540	460
BL-THS film-450	850.7	370, 465, 620	415, 520

for detailed calculations†). The calculated results show that three peaks at 597.7, 448.3 and 358.6 nm are supposed to appear in the reflection spectrum when the m value is taken as 3, 4, and 5, respectively, which conforms basically to the measured reflectance peak positions that locate at around 620, 465 and 370 nm, respectively.

The absorption properties of the THH and THS films were also investigated. To exclude the influence of ITO substrates, an ITO glass without TiO_2 coating that undergone the same calcination treatment was selected for UV-vis absorption measurements simultaneously. Fig. 7 shows the UV-vis absorption spectra of the calcined ITO and the TiO_2 films prepared from 150 nm PS film templates, where ITO glass and the three TiO_2 samples all display typical absorption curves of wide bandgap SnO_2 and TiO_2 semiconductors with the corresponding intrinsic absorption peaks at ~350 and 365 nm, respectively. However, for the thicker TiO_2 films with larger sphere sizes, an anomalous absorption in the visible-light region was found. From Fig. 8 and Table 1, it can be seen that in addition to typical intrinsic UV band absorption, a broad peak appears in the spectrum of each TiO_2 film from 450 nm PS templates, such as the absorption peak at 390 nm for ML THH film-450, 425 nm for BL THH film-450, 460 nm for ML THS film-450 and 520 nm for BL THS film-450, which imply a gradual red shift of the absorption peak position with increasing film thickness. As generally admitted, TiO_2 with wide bandgap energy (3.2 eV) can only be excited by UV light <~385 nm, except being modified with some dopants such as metals (Pt, Au)[26,35] and nonmetal

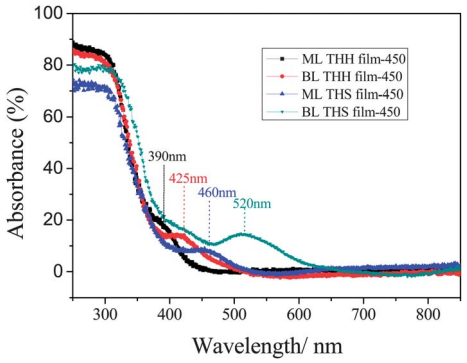

Fig. 8 UV-vis absorption spectra of THS and THS films obtained from 450 nm PS film templates.

elements (N, C)[2,36] that can narrow the band gap of TiO_2. Though carbon-containing PS templates were involved in the TiO_2 film preparation, it is believed that carbon element can be removed completely under atmosphere in the presence of O_2, and it has no contribution to visible light absorption.[26] Moreover, other TiO_2 films prepared from 150 nm PS templates through the same synthetic procedures did not show such visible light absorption (Fig. 7). Therefore, this anomalous absorption should be attributed to the structures of THH and THS films. We think this may be resulted from light extinction caused by THS film interference. According to eqn (2), when the m value is taken as follows,

$$m\lambda_{max} = 2n_{avg}d \ (m = 0.5, 1.5, 2.5, 3.5, \ldots) \quad (2)$$

the incident lights with λ satisfying eqn (2) can be quenched by their reflected lights from the TiO_2 films because the phase difference of the incident and reflected lights is half wavelength. Taking BL THS film-450 for instance as well for a calculation, when m is taken as 3.5 and 4.5, the lights with wavelengths of 512.3 and 398.5 nm will be quenched in theory (see S1 for calculation†). The calculated peak positions agree basically with the measured result (Fig. 8 and Table 1). In addition, it can be easily deduced that at a given m value, the λ_{max} of quenched lights is proportional to the thickness of TiO_2 films. This suggests that for the thinner films produced from

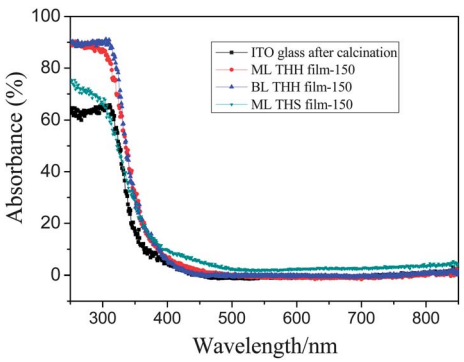

Fig. 7 UV-vis absorption spectra of ITO glass, and THS and THS films obtained from 150 nm PS film templates.

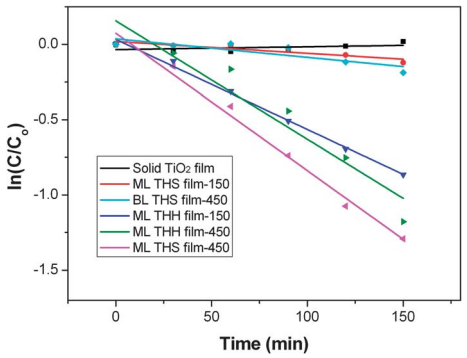

Fig. 9 The photocatalytic properties of THS and THS films as well as the solid TiO_2 film on ITO substrates.

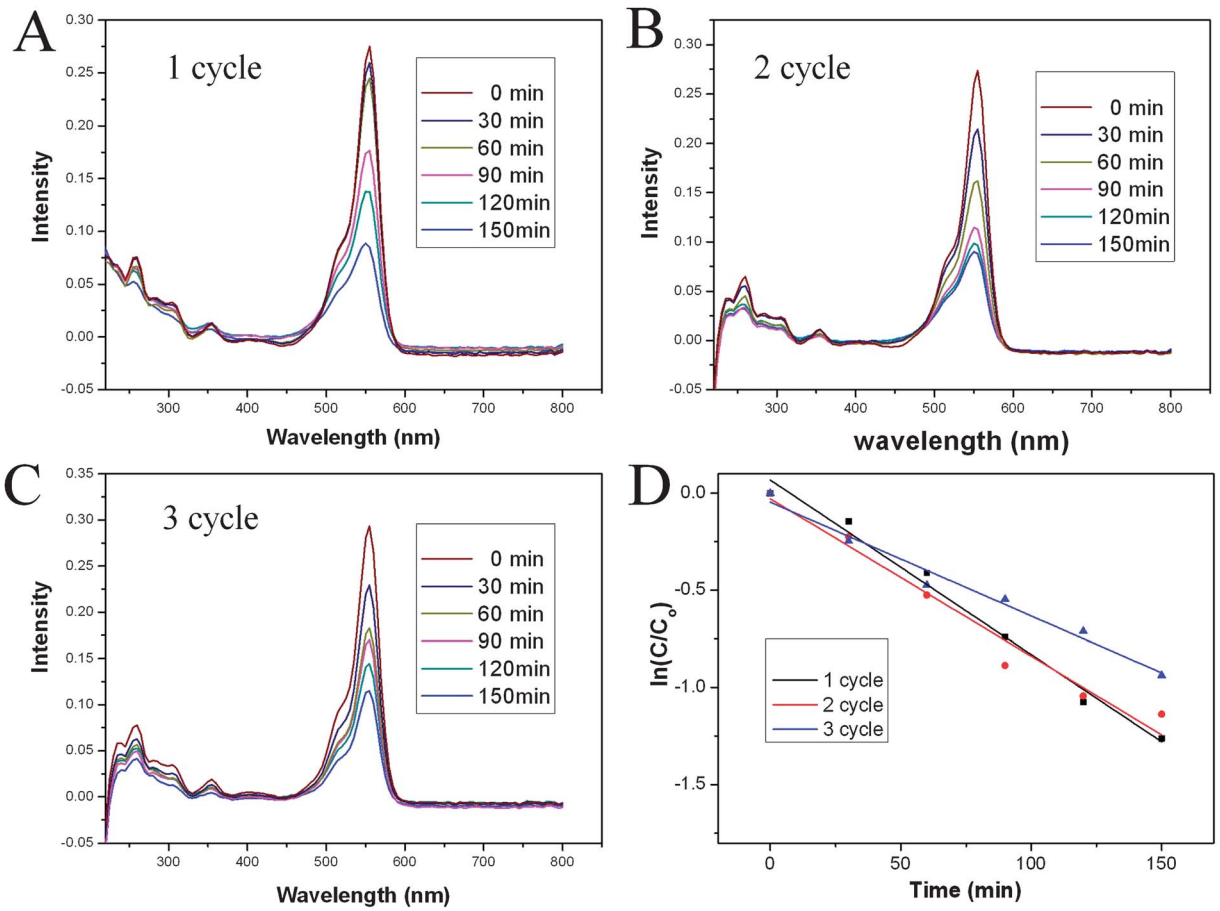

Fig. 10 Example of RhB degradation data with time under UV irradiation by ML THS film-450 at the first (A), second (B) and third cycles (C), and photocatalytic stability comparison of RhB degradation (ln(C/C_o) *versus* irradiation time) in the 3 cycles (D).

150 nm PS templates, light extinction occurs at shorter wavelengths in the UV-band. The extinction in this waveband is superpositioned with their strong intrinsic absorption and becomes invisible.

The prepared THH and THS films as well as the solid TiO_2 film were further investigated for their photocatalytic properties through RhB degradation under irradiation of a Hg lamp (300 W). It is noted that all the samples are normalized to the same area (1.4 cm × 1.4 cm) on ITO substrates. The photocatalytic properties of these samples are demonstrated in Fig. 9. The results show that all the THH and THS films present better performance than the solid TiO_2 film, which is probably due to the hollow structure of the THH and THS films that can facilitate diffusion kinetics in the photocatalytic processes. For the monolayer THH/THS films, it is found that the films consisting of larger sized THHs or THSs show higher catalytic efficiencies, for example, ML THS film-450 and ML THH film-450, which have similar performances, show faster degradation rates than ML THH film-150 and ML THS film-150. This may be attributed to the much improved diffusion kinetics in 450 nm THH/THS films because wider and more direct pathways can be provided, relative to 150 nm counterparts, for RhB molecules to dynamic adsorption/desorption on the films. It can also be seen that BL THS film-450 shows poor photocatalytic properties. We think this is likely resulted from its strong and wide-band light reflectance, which reduces its light harvesting property. In fact, photocatalysis is a complex process which involves many key factors related to both dynamics and thermodynamics. Since ML THS film-450 exhibits the highest photocatalytic activity, it is therefore selected as a recyclable catalyst for further RhB photocatalytic degradation. As shown in Fig. 10, photocatalytic measurements conducted in the first three cycles provided very similar degradation curves (Fig. 10A–C), though there is little deterioration with cycling (Fig. 10D), indicating a comparable efficiency and better photocatalytic stability of the sample.

4 Conclusions

In summary, ordered monolayer/bilayer THH and THS films with controlled structures and thickness have been successfully prepared from PS film templates through two different TiO_2 coating processes coupled with a designed template removal program. The prepared TiO_2 films exhibit tunable wide-band visible-light reflection (380 to 850 nm) and absorption (390 to 520 nm). The detailed mechanisms including reflection and absorption related to the structures of the THH and THH films have been discussed in conjunction with the calculation according to Bragg's law. The result is beneficial for not only

recognizing in depth the correlations between structures and properties of the nanostructured films, but also optimizing properties and performance of the film based devices through predesign. The prepared THH and THS films with good crystallinity, precisely controlled structures and novel optical properties have great potential in a variety of fields, such as efficient oxide electrodes[17,20] or scattering layers[18] for solar cells, recyclable catalysts for photocatalysis,[37] gas-permeable electrode materials for high-performance sensors,[38] and so on. In addition, this facile, convenient and controllable synthetic method can be further applied to other semiconductors, metals or their hybrid materials for high-quality monolayer/bilayer film preparation with expectable properties.

Acknowledgements

This work was financially supported by National Natural Science Foundation (21001082, 21273161 and 21101117), Shanghai Innovation program (13ZZ026), Scientific Research Foundation for the Returned Overseas Chinese Scholars of SEM, Shanghai Pujiang Program (10PJ1410400), Visiting scholar fund of the Key Laboratory for Ultrafine Materials of Ministry of Education, East China University of Science and Technology, Research Fund for the Doctoral Program of Higher Education of China (20090072120013) and the Fundamental Research Funds for the Central Universities.

References

1 A. Fujishima and K. Honda, *Nature*, 1972, **238**, 37.
2 R. Asahi, T. Morikawa, T. Ohwaki, K. Aoki and Y. Taga, *Science*, 2001, **293**, 269.
3 H. G. Yang, C. H. Sun, S. Z. Qiao, J. Zou, G. Liu, S. C. Smith, H. M. Cheng and G. Q. Lu, *Nature*, 2008, **453**, 638.
4 B. Oregan and M. Grätzel, *Nature*, 1991, **353**, 737.
5 B. Liu and E. S. Aydil, *J. Am. Chem. Soc.*, 2009, **131**, 3985.
6 X. J. Feng, K. Shankar, O. K. Varghese, M. Paulose, T. J. Latempa and C. A. Grimes, *Nano Lett.*, 2008, **8**, 3781.
7 J. F. Ye, W. Liu, J. G. Cai, S. Chen, X. W. Zhao, H. H. Zhou and L. M. Qi, *J. Am. Chem. Soc.*, 2011, **133**, 933.
8 J. S. Chen, Z. Y. Wang, X. C. Dong, P. Chen and X. W. Lou, *Nanoscale*, 2011, **3**, 2158; Z. M. He, G. H. Guai, J. Liu, C. X. Guo, J. S. C. Loo, C. M. Li and T. T. Y. Tan, *Nanoscale*, 2011, **3**, 4613; T. Chen, W. H. Hu, J. L. Song, G. H. Guai and C. M. Li, *Adv. Funct. Mater.*, 2012, **22**, 5245; G. H. Guai, Y. Li, C. M. Ng, C. M. Li and M. B. Chan-Park, *ChemPhysChem*, 2012, **13**, 2566.
9 I.-D. Kim, A. Rothschild, B. H. Lee, D. Y. Kim, S. M. Jo and H. L. Tuller, *Nano Lett.*, 2006, **6**, 2009.
10 O. K. Varghese, D. Gong, M. Paulose, K. G. Ong and C. A. Grimes, *Sens. Actuators, B*, 2003, **93**, 338.
11 X. T. Zhang, O. Sato, M. Taguchi, Y. Einaga, T. Murakami and A. Fujishima, *Chem. Mater.*, 2005, **17**, 696.
12 I. P. Parkin and R. G. Palgrave, *J. Mater. Chem.*, 2005, **15**, 1689.
13 B. Peng, F. Q. Tang, D. Chen, X. L. Ren, X. W. Meng and J. Ren, *J. Colloid Interface Sci.*, 2009, **329**, 62.
14 H. C. Choi, Y. M. Jung and S. B. Kim, *Vib. Spectrosc.*, 2005, **37**, 33.
15 G. K. Mor, S. Kim, M. Paulose, O. K. Varghese, K. Shankar, J. Basham and C. A. Grimes, *Nano Lett.*, 2009, **9**, 4250.
16 G. Subramania, Y. J. Lee, A. J. Fischer and D. D. Koleske, *Adv. Mater.*, 2010, **22**, 487.
17 S. C. Yang, D. J. Yang, J. Kim, J. M. Hong, H. G. Kim, I.-D. Kim and H. Lee, *Adv. Mater.*, 2008, **20**, 1059.
18 L. Song, H. Bin Yang, X. Wang, S. Y. Khoo, C. C. Wong, X. W. Liu and C. M. Li, *ACS Appl. Mater. Interfaces*, 2012, **4**, 3712.
19 Y. Z. Li, T. Kunitake and S. Fujikawa, *J. Phys. Chem. B*, 2006, **110**, 13000.
20 S. Nishimura, N. Abrams, B. A. Lewis, L. I. Halaoui, T. E. Mallouk, K. D. Benkstein, J. V. D. Lagemaat and A. J. Frank, *J. Am. Chem. Soc.*, 2003, **125**, 6306.
21 S. Guldin, S. Hüttner, M. Kolle, M. E. Welland, P. Müller-Buschbaum, R. H. Friend, U. Steiner and N. Tétreault, *Nano Lett.*, 2010, **10**, 2303.
22 H. Hen, S. Chen, X. Quan and Y. B. Zhang, *Environ. Sci. Technol.*, 2010, **44**, 451.
23 J. I. L. Chen, G. V. Freymann, V. Kitaev and G. A. Ozin, *J. Am. Chem. Soc.*, 2007, **129**, 1196.
24 C. W. Cheng, S. K. Karuturi, L. J. Liu, J. P. Liu, H. X. Li, L. T. Su, A. I. Y. Tok and H. J. Fan, *Small*, 2012, **8**, 37.
25 J. B. Joo, Q. Zhang, I. Lee, M. Dahl, F. Zaera and Y. D. Yin, *Adv. Funct. Mater.*, 2012, **22**, 166.
26 Y. Z. Jiao, C. X. Peng, F. F. Guo, Z. H. Bao, J. H. Yang, L. Schmidt-Mende, R. Dunbar, Y. Qin and Z. F. Deng, *J. Phys. Chem. C*, 2011, **115**, 6405; H. C. Pang, H. B. Yang, C. X. Guo, J. L. Lu and C. M. Li, *Chem. Commun.*, 2012, **48**, 8832.
27 S. Q. Shang, X. L. Jiao and D. R. Chen, *ACS Appl. Mater. Interfaces*, 2012, **4**, 860.
28 L. J. Liu, S. K. Karuturi, L. T. Su and A. I. Y. Tok, *Energy Environ. Sci.*, 2011, **4**, 209.
29 C. Li, G. S. Hong, P. W. Wang, D. P. Yu and L. M. Qi, *Chem. Mater.*, 2009, **21**, 891.
30 C. Li, G. S. Hong and L. M. Qi, *Chem. Mater.*, 2010, **22**, 476.
31 J. Rybczynski, U. Ebels and M. Giersig, *Colloids Surf., A*, 2003, **219**, 1.
32 C. F. Blanford, R. C. Schroden, M. Al-Daous and A. Stein, *Adv. Mater.*, 2001, **13**, 26.
33 G. I. N. Waterhouse, J. B. Metson, H. Idriss and D. S. Waterhouse, *Chem. Mater.*, 2008, **20**, 1183.
34 K. Sumioka, H. Kayashima and T. Tsutsui, *Adv. Mater.*, 2002, **14**, 1284.
35 V. Subramanian, E. E. Wolf and P. V. Kamat, *J. Am. Chem. Soc.*, 2004, **126**, 4943.
36 E. M. Neville, M. J. Mattle, D. Loughrey, B. Rajesh, M. Rahman, J. M. D. MacElroy, J. A. Sullivan and K. R. Thampi', *J. Phys. Chem. C*, 2012, **116**, 16511.
37 S. W. Wang, Y. Yu, Y. H. Zuo, C. Z. Li, J. H. Yang and C. H. Lu, *Nanoscale*, 2012, **4**, 5895.
38 Y. Qin, F. Zhang, Y. Chen, Y. J. Zhou, J. Li, A. W. Zhu, Y. P. Luo, Y. Tian and J. H. Yang, *J. Phys. Chem. C*, 2012, **116**, 11994.

